(Received 23 January 2026, Accepted 7 March 2026, Scheduled 26 March 2026)

An Anti-Interrupted Sampling Repeater Jamming Method Based on SSFA-MCPC Waveform Design Combined with Segmented Mismatched Filtering

Ji Li[1], Hai Liu[2,*], and Wei Wang[1]

[1] College of Physics & Electronic Science, Changsha University of Science & Technology, Changsha 410114, China
[2] College of Computer Science and Technology, Changsha University of Science & Technology, Changsha 410076, China

ABSTRACT: Interrupted Sampling Repeater Jamming (ISRJ) is a typical intra-pulse coherent deceptive interference that poses a serious threat to radar target detection and tracking performance. This paper proposes an anti-jamming method that integrates a dual-modulated SSFA-MCPC waveform with a segmented mismatched filtering scheme. Based on the multi-carrier phase-coded (MCPC) signal, we apply random sub-pulse frequency agility and chaotic time-domain phase coding to design the SSFA-MCPC waveform. This design enhances the distinction between the radar signal and interference and improves the mutual masking among sub-pulses. To counter ISRJ, a segmented mismatched filtering algorithm is proposed. Specifically, a bank of sub-pulse matched filters is constructed to perform segmented pulse compression on the received echoes, and the Otsu algorithm is employed to adaptively identify jammed sub-pulses. Finally, a reconstructed mismatched filter is applied to suppress interference. Simulation results demonstrate that the proposed method does not rely on prior knowledge of the jamming parameters and can effectively suppress ISRJ under three different forwarding modes. Compared with existing methods, the proposed approach has lower computational complexity and shows strong potential for practical engineering applications.

1. INTRODUCTION

In modern electronic warfare environments, radar systems are confronted with increasingly complex scenarios. With the widespread application of digital radio frequency memory (DRFM) technology [1, 2], repeater jamming has emerged as a major threat owing to its flexible implementation and low dependence on radar parameters. Interrupted sampling repeater jamming (ISRJ), as a typical DRFM-based intra-pulse coherent deceptive interference [3], intercepts and retransmits radar signals to obtain partial pulse compression gain, generating dense false targets with both deceptive and suppressive effects. Owing to its flexible and diverse jamming patterns, ISRJ can severely degrade the radar target detection and tracking performance.

Conventional radar anti-jamming techniques, such as interpulse frequency agility [4, 5] and radio-frequency masking [6], are ineffective for ISRJ. Furthermore, when interference enters the main lobe, traditional spatial-domain methods fail to provide sufficient suppression [7]. Consequently, effective countermeasures against ISRJ are urgently needed. Existing ISRJ countermeasures can be broadly classified into two categories: transmitter-side waveform design and receiver-side signal processing. The first category, commonly referred to as active anti-jamming strategies, mainly focuses on transmitter-side waveform design and joint transmitting-receiving waveform optimization. In [8, 9], linear frequency-modulated (LFM) waveforms with an intra-pulse stepped frequency and intra-pulse Costas frequency stepping were proposed to counter ISRJ. In [10], an intra-pulse orthogonal LFM phase-coded waveform was designed to reduce the signal-interference correlation. A novel Electronic Counter-Countermeasures (ECCM) scheme based on an intra-pulse dual-parameter agile radar waveform design and fractional Fourier transform (FrFT) was proposed in [11]. In [12], a method for countering ISRJ based on a complementary code design was introduced. The work in [13–15] focused on a multi-carrier phase-coded radar waveform design to enhance the anti-jamming performance of the waveform. Additionally, joint transmitting-receiving waveform design has also been investigated as an effective ISRJ suppression strategy. In [16–18], the optimization design of joint transmitting waveforms and receiving filters was studied to suppress interference while maintaining low sidelobe levels after pulse compression. However, such optimization approaches involve high computational complexity and are difficult to implement in real-time radar signal-processing systems.

The second category, referred to as passive anti-jamming strategies, mainly includes interference reconstruction and filtering. In [19], a joint "interference perception-parameter estimation-interference suppression" approach for ISRJ countermeasures was proposed. In [20], a reconstruction cancellation approach was developed using time-frequency analysis and deconvolution to estimate and reconstruct the interference signal, followed by cancellation. In [21], ISRJ was identified by analyzing the time-frequency distribution differences

* Corresponding author: Hai Liu (isliuhai@163.com).

between target echoes and interference after pulse compression, followed by filtering to suppress the interference. In [22], ISRJ identification and suppression were achieved by analyzing peak feature differences in the ambiguity function of phase-coded signals, followed by Doppler compensation and filtering. In [23], a short-time fractional Fourier transform (STFrFT) was applied to analyze intra-pulse frequency-agile signals, and image-processing techniques were used to remove interference. In [24], a waveform-domain adaptive matched filtering method was proposed for ISRJ suppression. In [25], ISRJ suppression was achieved by separating the interference and target components using an undersampling-based blind source separation method.

In summary, although existing methods can effectively counter ISRJ, they often suffer from high computational complexity, poor real-time performance, or strong dependence on the accurate prior knowledge of jamming parameters. Furthermore, most ISRJ countermeasures are based on LFM waveforms and their variants, whereas relatively little attention has been devoted to ISRJ suppression using MCPC signals. Compared with LFM waveforms, MCPC signals exhibit more balanced performance in terms of ambiguity sidelobe suppression, envelope fluctuation control, and spectral efficiency, thereby offering an enhanced low probability of intercept and anti-jamming capability [26]. However, existing MCPC-based studies have mainly focused on waveform design, with limited consideration of receiver-side processing. Motivated by these observations and practical radar engineering requirements, this paper proposes a combined active-passive anti-jamming approach based on SSFA-MCPC (Segmented Subcarrier Frequency Agility Multi-carrier Chaotic Phase Code) waveform design and segmented mismatched filtering.

Considering the discontinuous and periodic sampling characteristics of ISRJ, the proposed SSFA-MCPC waveform is generated as follows. First, a chaotic phase code is applied in the time domain. The coded sequence is then partitioned into equal-length segments, each modulating a distinct subcarrier. Finally, intra-pulse frequency agility is realized by randomly hopping the carrier frequency of each segment. This design increases the discrepancy between target echoes and ISRJ, enhances mutual masking among sub-pulses, and mitigates the high peak-to-average power ratio of conventional MCPC signals. Based on this waveform, an ISRJ suppression method combining segmented pulse compression and mismatched filtering is developed. Specifically, a bank of sub-pulse matched filters is constructed to perform segmented pulse compression on the received echoes. The Otsu algorithm is then employed to adaptively identify jammed sub-pulses based on their pulse compression peaks, followed by mismatched filtering to suppress interference.

The remainder of this paper is organized as follows. The principles of the various ISRJ modes are introduced in Section 2. Section 3 establishes the signal model including the SSFA-MCPC signal design and its corresponding ambiguity function. In Section 4, the ISRJ suppression method is introduced, detailing segmented pulse compression processing, Otsu-based ISRJ identification and suppression, and the algorithm flow of segmented mismatched filtering for anti-jamming. The simulation results are presented in Section 5. Finally, the conclusions are summarized in Section 6.

2. PRINCIPLE OF ISRJ

ISRJ employs a DRFM jammer to intermittently sample and rapidly retransmit intercepted radar signals, thereby generating multiple coherent replicas of the radar waveform. Dense false targets can be produced at the receiver by exploiting the matched filtering property of the pulse-compression radars. After pulse compression, the coherent retransmitted signals yield a high processing gain, resulting in both deceptive and suppressive jamming effects. The working principle of the ISRJ is illustrated in Fig. 1.

According to different forwarding patterns, ISRJ can be generally classified into three types: Interrupted Sampling Direct Repeater Jamming (ISDRJ), Interrupted Sampling Periodic Repeater Jamming (ISPRJ), and Interrupted Sampling Cyclic Repeater Jamming (ISCRJ). Different forwarding modes lead to distinct jamming effects and correspond to different operating modes of the jammer. Assuming that the jammer performs synchronous sampling, the forwarding delay is zero. The radar transmission signal is expressed as $s(t)$, with a pulse width of T_p. N denotes the number of sampled pulses; τ denotes the jammer sampling duration; T_j denotes the jammer sampling period.

The ISDRJ immediately forwards the current segment after sampling the signal within each sampling period. This can be expressed as:

$$J_{\text{ISDRJ}}(t) = \sum_{n=0}^{N-1} \text{rect}\left(\frac{t - nT_j - \tau}{\tau}\right) s(t-\tau) \tag{1}$$

The ISPRJ repeatedly forwards the current sampling segment after sampling the signal within the sampling period, does not stop forwarding until the beginning of the next sampling period, and performs a new round of sampling and forwarding operations. The number of repeated forwardings is given by $K = \lfloor T_j/\tau \rfloor - 1$, and the jamming signal can be expressed as:

$$J_{\text{ISPRJ}}(t) = \sum_{k=1}^{K} \sum_{n=0}^{N-1} \text{rect}\left(\frac{t - nT_j - k\tau}{\tau}\right) s(t-k\tau) \tag{2}$$

The ISCRJ samples and stores the signal within each sampling period. In addition to forwarding the sampling segments within the current sampling period, it also forwards all previously stored sampling segments in the reverse order. The number of cyclic forwarding times is given by $R = \min\{K, N\}$, where $N = \lfloor T_p/T_j \rfloor$. The jamming signal can be expressed as:

$$J_{\text{ISCRJ}}(t) = \sum_{k=1}^{K} \sum_{r=1}^{R-1} \text{rect}\left(\frac{t - rT_j - k\tau}{\tau}\right) s\left(t - (k-1)T_j - k\tau\right) \tag{3}$$

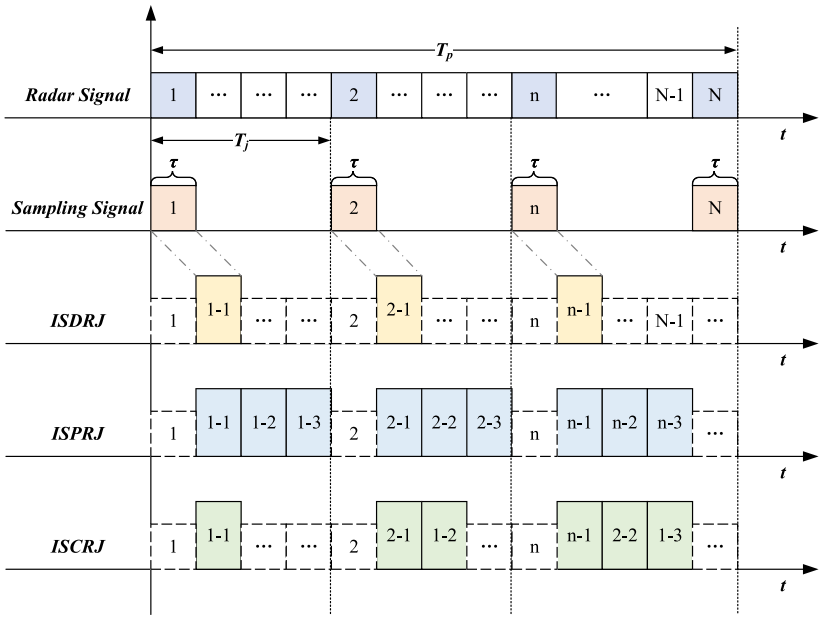

FIGURE 1. The working principle of ISRJ.

3. SIGNAL MODEL

3.1. SSFA-MCPC Signal Model

To enhance the anti-jamming capability of radar, a novel radar signal termed SSFA-MCPC is proposed from the perspective of waveform design. In the time domain, a logistic chaotic sequence with favorable pseudo-randomness and autocorrelation properties is employed to perform phase-coding modulation on each symbol of the MCPC signal. In the frequency domain, the concept of frequency agility is introduced by extracting equal-length code segments from the MCPC signal to form sub-pulses, and random intra-pulse frequency agility of each segmented sub-pulse across different subcarrier frequencies is achieved through frequency-coding modulation. As a result, the proposed signal exhibits noise-like characteristics within a pulse and low inter-pulse correlation, making it resistant to ISRJ. The complex envelope of the SSFA-MCPC signal transmitted by the radar can be expressed as:

$$\begin{aligned} s(t) &= \sum_{p=1}^{P} w_p u_p(t) \exp\left(j2\pi f_p t\right) \\ &= \sum_{p=1}^{P} \sum_{m=1}^{M} w_p \alpha_{p,m} \exp\left[j2\pi b(p)\Delta f t\right] \\ &\quad \operatorname{rect}\left(\frac{t-(p-1)T_{sub}-(m-1)t_b}{t_b}\right) \end{aligned} \tag{4}$$

where P represents the number of subcarriers; $w_p = |w_p|e^{j\varphi_p}$ is the complex weighting factor on the pth subcarrier, where $|w_p|$ and φ_p denote the frequency weighting amplitude and phase, respectively; $u_p(t)$ is the complex envelope of the pth subcarrier signal; $f_p = b(p)\Delta f$ is the pth subcarrier frequency, where $b(p)$ is the frequency modulation code of the pth subcarrier, and $\Delta f = 1/t_b$ represents the subcarrier frequency interval; t_b is the duration of a single code chip. M denotes the number of code chips in each segmented sub-pulse, and $\alpha_{p,m}$ represents the phase coding of the mth code chip on the pth subcarrier. $\operatorname{rect}(x)$ is a rectangular envelope pulse with the value $1(0 \le x \le 1)$ or 0(otherwise). $T_{sub} = M * t_b$ denotes the duration of each segmented sub-pulse. The signal bandwidth and pulse duration are $B = P\Delta f$ and $T_p = PT_{sub}$, respectively. The time-frequency structure of the SSFA-MCPC signal is illustrated in Fig. 2.

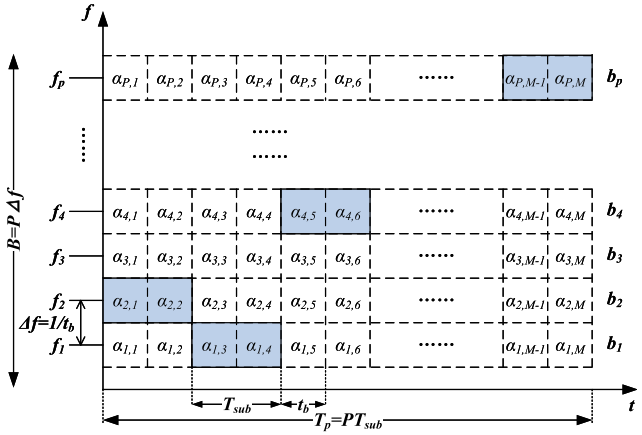

FIGURE 2. Time-frequency structure of the SSFA-MCPC signal.

As shown in Fig. 2, compared with the conventional MCPC signal, the proposed SSFA-MCPC signal introduces an additional modulation dimension, endowing the waveform with two-dimensional modulation agility and optimization capability, which enhances its randomness and unpredictability. Owing to the flexible variation of the sub-pulse frequencies and phase coding patterns, the proposed waveform exhibits a supe-

rior low probability of intercept performance. Moreover, owing to the discontinuous sampling nature of ISRJ, the jammer cannot acquire the complete time-frequency characteristics of the radar signal, thereby enlarging the discrepancy between the radar signal and ISRJ interference, and reducing the impact of jamming sidelobes. The segmented sub-pulses are orthogonal in both the time and frequency domains, enabling effective mutual masking and facilitating subsequent anti-jamming processing.

Assuming that there is a scattering point target in the radar scenario at distance R, the target echo signal can be expressed as:

$$\begin{aligned} s_r(t) &= As(t-\Delta t) \\ &= A\sum_{p=1}^{P}\sum_{m=1}^{M} w_p\alpha_{p,m}\exp\left[j2\pi f_p(t-\Delta t)\right] \\ &\quad \text{rect}\left(\frac{t-\Delta t-(p-1)T_{sub}-(m-1)t_b}{t_b}\right) \end{aligned} \tag{5}$$

where A is the target amplitude, $\Delta t = 2R/c$ the target echo delay, and c the speed of light. Let the distance between the jammer and the radar be R_j. The interrupted sampling repeater jamming signal can be described as follows:

$$\begin{aligned} s_j(t) &= A_j\sum_{k=1}^{K}\sum_{n=0}^{N-1}\text{rect}\left(\frac{t-nT_j-k\tau-\Delta t_j}{\tau}\right) \\ &\quad s\left(t-k\tau-\Delta t_j\right) \end{aligned} \tag{6}$$

where A_j represents the amplitude of the jamming signal, and $\Delta t_j = 2R_j/c$ is the jamming echo delay. Let $n(t)$ denote the additive Gaussian noise. The total echo signal received by the radar can then be expressed as

$$s_{echo}(t) = s_r(t) + s_j(t) + n(t). \tag{7}$$

3.2. Ambiguity Function of SSFA-MCPC Signal

To analyze the anti-jamming performance of the SSFA-MCPC signal, starting from the output of the matched filter, the ambiguity function can be calculated as follows:

$$\begin{aligned} \chi(\tau,f_d) &= \int_{-\infty}^{+\infty} s(t)s^*(t+\tau)e^{j2\pi f_d t}dt \\ &= \int_{-\infty}^{+\infty}\sum_{p=1}^{P}\sum_{l=1}^{P} w_p w_l^* u_p(t)u_l^*(t+\tau) \\ &\quad \exp(j2\pi f_p t)\exp[-j2\pi f_l(t+\tau)]e^{j2\pi f_d t}dt \\ &= \sum_{p=1}^{P}\sum_{l=1}^{P} w_p w_l^*\exp[-j2\pi f_l\tau]\int_{-\infty}^{+\infty} u_p(t) \\ &\quad u_l^*(t+\tau)\exp\left[j2\pi(f_p-f_l)t+j2\pi f_d t\right]dt \\ &= \chi_{auto}\left(\tau,f_d\right)+\chi_{cross}\left[\tau,f_p-f_l+f_d\right] \end{aligned} \tag{8}$$

where $f_p = b(p)\Delta f$ and $f_l = b(l)\Delta f$. χ_{auto} corresponds to the case $p = l$ and represents the main component of the ambiguity function, whereas χ_{cross} corresponds to the case $p \neq l$ and represents the sidelobe components of the ambiguity function. The final expression can be written as:

$$\begin{aligned} \chi_{auto}\left(\tau,f_d\right) &= \sum_{p=1}^{P}|w_p|^2 e^{\left[-j2\pi f_p\tau+j2\pi f_d(p-1)T_{sub}\right]} \\ &\quad \sum_{q=-(M-1)}^{M-1}\chi_u(\tau-qt_b,f_d) \\ &\quad \sum_{m=1}^{M}\alpha_{p,m}\alpha_{p,m+q}^* e^{\left[j2\pi f_d(m-1)t_b\right]} \end{aligned} \tag{9}$$

$$\begin{aligned} \chi_{cross}\left(\tau,f_d'\right) &= \sum_{p=1}^{P}\sum_{\substack{l=1\\ l\neq p}}^{P} w_p w_l^* e^{\left[-j2\pi f_l\tau+j2\pi f_d'(p-1)T_{sub}\right]} \\ &\quad \sum_{q=i}^{i+l}\chi_u\left(\tau-(l-q)T_{sub}-qt_b,f_d'\right) \\ &\quad \sum_{m=1}^{M}\alpha_{p,m}\alpha_{l,m+q}^* e^{\left[j2\pi f_d'(m-1)t_b\right]} \end{aligned} \tag{10}$$

$$\chi_u\left(\tau,f_d\right) = \begin{cases} e^{\left[j\pi f_d(t_b-\tau)\right]}\frac{\sin[\pi f_d(t_b-|\tau|)]}{\pi f_d(t_b-|\tau|)} \\ \qquad \times\left(1-\frac{|\tau|}{t_b}\right), & |\tau|\leq t_b \\ 0, & |\tau|>t_b \end{cases} \tag{11}$$

where $f_d' = f_p - f_l + f_d$ and $i = \lfloor\tau/t_b\rfloor$. $\chi_u(\tau,f_d)$ is the ambiguity function of the rectangular envelope pulse, $\text{rect}(t/t_b)$. It can be seen that the ambiguity function of the SSFA-MCPC signal is essentially obtained through translation and modulation of $\chi_u(\tau,f_d)$, as illustrated in Fig. 3.

As shown in Fig. 3, the ambiguity function of the SSFA-MCPC signal exhibits a thumbtack-like shape, with a relatively

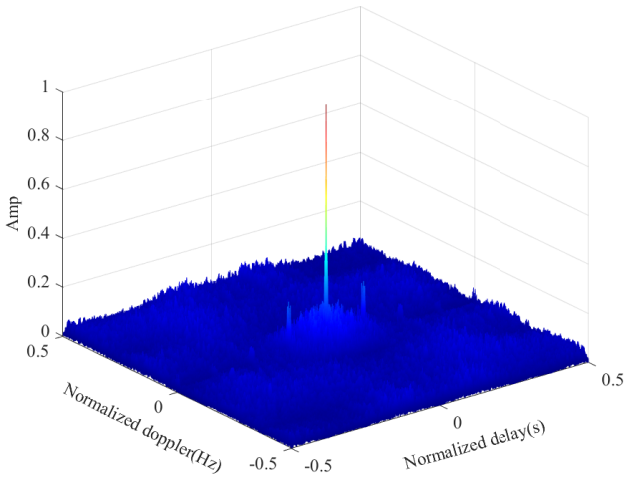

FIGURE 3. Three-dimensional ambiguity figure of SSFA-MCPC signal.

flat time-frequency distribution and only a single dominant central peak. Compared with the "slanted ridge" ambiguity function of the LFM signal [27], the thumbtack-shaped ambiguity function is free of range-Doppler coupling and features lower sidelobe levels. Consequently, the SSFA-MCPC signal provides a higher measurement accuracy and superior target detection capability.

4. ISRJ SUPPRESSION METHOD

Based on an analysis of the ISRJ principle, it is found that jamming exhibits discontinuous sampling characteristics in the time domain, such that the radar signal can only be partially sampled in segments. Therefore, the segmented sub-pulses of the SSFA-MCPC signal designed in this study can provide mutual masking. Specifically, when jammer sampling is synchronized with signal segmentation, if one segment is sampled by the jammer, another segment is not sampled, which can be regarded as one segment masking the other. By exploiting this masking effect and the orthogonality of the waveforms, processing the received echoes using unsampled signals provides a feasible solution for ISRJ suppression and target parameter extraction.

4.1. Segmented Pulse Compression Processing

Pulse compression is a classical method used in radar signal processing. Owing to the flexible structure of the SSFA-MCPC signal, its pulse-compression schemes also exhibit diverse characteristics. Different from conventional matched-filter-based pulse compression, according to the orthogonality and random variation of sub-pulses in the time-frequency domain, a segmented pulse compression method is adopted in this study to classify and identify the jammed sampled sub-pulses.

Specifically, the transmitted signal $s(t)$ is segmented into P parts by time-delay truncation according to the sub-pulse duration. Each segment is randomly coded in the time domain, and the spectrum is randomly distributed over different subcarriers. The time-domain expression of the pth segmented sub-pulse signal is given by:

$$s_{t\_sub}(t,p) = \text{rect}\left(\frac{t-(p-1)T_{sub}}{T_{sub}}\right) s(t) \tag{12}$$

Then, the time-domain impulse response of the matched filter corresponding to the pth sub-pulse is given by $h(t,p) = s^*_{t\_sub}(-t,p)$, which is equivalent to decomposing the original single wideband matched filter into a bank of P sub-pulse narrowband matched filters. These filters perform pulse compression on the received echo signal separately, and the pulse compression output corresponding to the pth sub-pulse matched filter is expressed as:

$$\begin{aligned} y(t,p) &= s_{echo}(t) \otimes h(t,p) \\ &= [s_r(t) + s_j(t) + n(t)] \otimes s^*_{t\_sub}(-t,p) \end{aligned} \tag{13}$$

4.2. Otsu-Based ISRJ Identification and Suppression

Owing to the intermittent sampling and delayed forwarding characteristics of the jammer, only part of the transmitted signal is sampled and retransmitted. Therefore, when the signal is divided into multiple sub-pulses, these sub-pulses can be classified into jammed sampled sub-pulses and unjammed sub-pulses. After the jammer samples a sub-pulse, it retransmits this sub-pulse, so the received echo contains not only the target echo but also the retransmitted sampled sub-pulse segments. Consequently, the sampled sub-pulses exhibit a higher coherent processing gain after matched filtering.

Moreover, to achieve deceptive and suppressive effects, the jamming energy should be generally much higher than the target energy. Consequently, after segmented pulse compression, the jammed sampled sub-pulses and unjammed sub-pulses can be distinguished by their pulse compression peak values, where the sampled sub-pulses produce higher peaks than the unsampled ones. Based on the difference in peak magnitudes, the Otsu algorithm is employed to classify and identify whether a sub-pulse is affected by jamming.

Otsu is a classical adaptive thresholding method. It automatically determines the optimal threshold by maximizing the between-class variance, such that the two segmented classes achieve maximum separability [28]. Therefore, this study first computes the peak values of all sub-pulses after matched filtering. The Otsu algorithm is then applied to obtain the optimal threshold for these peaks. This threshold is used to identify whether each sub-pulse is sampled by the jammer. Finally, the mismatched filter is reconstructed to achieve jamming suppression. The detailed procedure is as follows.

Step 1: Let the peak value of the echo signal after pulse compression using the pth $(p = 1, 2, \ldots, P)$ sub-pulse matched filter be denoted as $peak(p)$. The interval between the minimum and maximum values of $peak(p)$ is evenly divided into I subintervals. Each $peak(p)$ falling into the ith $(i = 1, 2, \ldots, I)$ interval is quantized as ξ_i, which represents the center value of the ith interval. Let m_i denote the number of $peak(p)$ values within the ith interval.

Step 2: The probability of occurrence of the quantized value ξ_i is calculated as:

$$p(\xi_i) = \frac{m_i}{P}, \quad i = 1, 2, \ldots, I. \tag{14}$$

Step 3: Assume that the quantized value of the ηth interval is ξ_η. The quantized values obtained in Step 1 are then divided into two sets:

$$A = \{\xi_i \le \xi_\eta\}, \quad B = \{\xi_i > \xi_\eta\}. \tag{15}$$

The occurrence probabilities of sets A and B are calculated as:

$$P_A(\eta) = \sum_{i=1}^{\eta} p(\xi_i), \quad P_B(\eta) = \sum_{i=\eta+1}^{I} p(\xi_i), \tag{16}$$

where $P_A(\eta) + P_B(\eta) = 1$.

Step 4: The mean values of the two sets are given by:

$$\mu_A(\eta) = \frac{1}{P_A(\eta)} \sum_{i=1}^{\eta} \xi_i p(\xi_i)$$

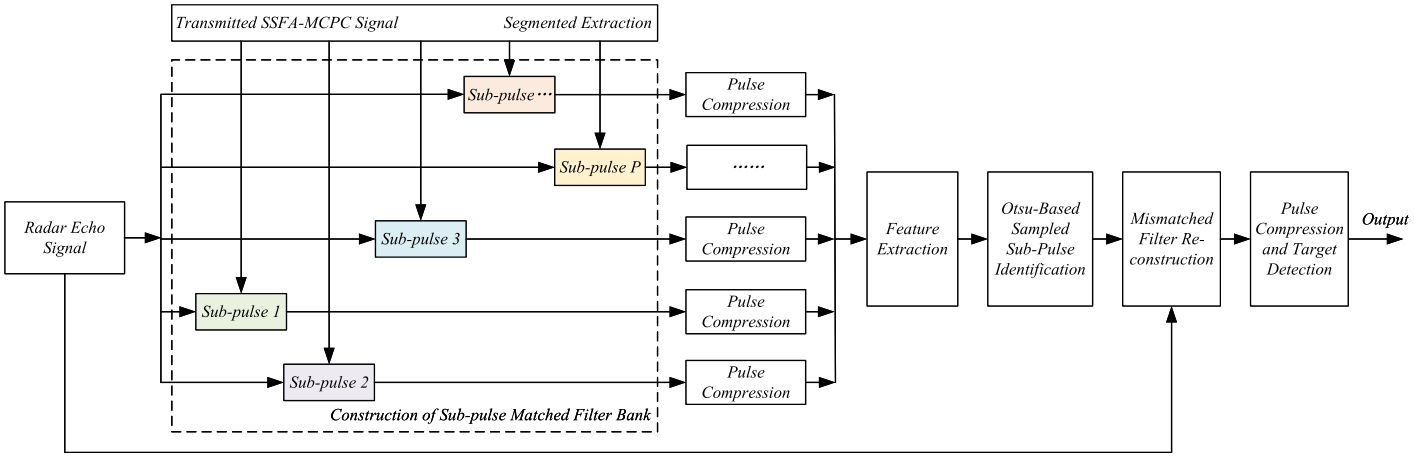

FIGURE 4. Flowchart of the segmented mismatched filtering anti-jamming algorithm based on the SSFA-MCPC signal.

$$\mu_B(\eta) = \frac{1}{P_B(\eta)} \sum_{i=\eta+1}^{I} \xi_i p(\xi_i) \tag{17}$$

Step 5: The between-class variance corresponding to threshold ξ_η is defined as:

$$\sigma^2(\xi_\eta) = P_A(\eta) P_B(\eta) \left[\mu_A(\eta) - \mu_B(\eta)\right]^2 \tag{18}$$

By searching over $\eta = 1, 2, \ldots, I$, the optimal threshold ξ_η^* is determined by maximizing the between-class variance,

$$\xi_\eta^* = \arg \max_{\xi_i \le \xi_\eta \le \xi_I} \sigma^2(\xi_\eta) \tag{19}$$

The optimal threshold is then used to identify the jammer-sampled sub-pulses.

Sub-pulses with peak values lower than the threshold are identified as unjammer-sampled sub-pulses, whereas sub-pulses with peak values higher than the threshold are identified as jammer-sampled sub-pulses. The matched filters corresponding to the identified jammer-sampled sub-pulses are removed. The remaining filters are reconstructed to form a new mismatched filter, which is then applied to the received echo for pulse compression to achieve jamming suppression. At this stage, the time-domain impulse response of the sub-pulse matched filter is given by:

$$h'(t,p) = s'^{*}_{t\_sub}(-t,p) = \begin{cases} 0, & peak(p) \ge \xi_\eta^* \\ s^*_{t\_sub}(-t,p), & peak(p) < \xi_\eta^* \end{cases} \tag{20}$$

Accordingly, the overall reconstructed mismatched filter against jamming can be expressed as:

$$h'(t) = \sum_{p=1}^{P} h'(t,p) = \sum_{p=1}^{P} s'^{*}_{t\_sub}(-t,p) \tag{21}$$

The received echo is then pulse-compressed using the reconstructed filter to suppress the ISRJ, which can be written as:

$$y'(t) = s_{echo}(t) \otimes h'(t) \tag{22}$$

4.3. Algorithm Flow of the Segmented Mismatched Filtering Anti-Jamming

As analyzed in Subsections 4.1 and 4.2, the flowchart of the SSFA-MCPC signal combined with the segmented mismatched filtering anti-jamming algorithm is illustrated in Fig. 4. The detailed implementation procedure is summarized as follows.

1. The radar receives the echo signal and down-converts it to a baseband signal.
2. The transmitted SSFA-MCPC signal is segmented by time-delay truncation to form sub-pulse signals, and a bank of P sub-pulse narrowband matched filters is constructed.
3. The received echo signal is processed using the filter bank. Segmented pulse compression is performed for each sub-pulse in parallel to improve the processing speed, yielding pulse compression outputs corresponding to the P sub-pulse matched filters.
4. Based on the peak characteristics of the pulse compression outputs, the optimal threshold is adaptively determined using the Otsu algorithm, enabling the identification of the jammer-sampled sub-pulses. The matched filters corresponding to the identified jammer-sampled sub-pulses are removed to construct a mismatched filter against jamming.
5. The reconstructed mismatched filter is applied to the received echo for pulse compression to achieve jamming suppression. Based on the principles of orthogonality and mutual masking, unsampled signal components are exploited to extract and detect radar target parameters.

5. SIMULATION ANALYSIS

To verify the effectiveness of the proposed anti-jamming method based on the SSFA-MCPC signal combined with segmented mismatched filtering, several simulation comparison experiments were designed to perform interference suppression and performance evaluation for three typical types of ISRJ. It was assumed that there was a moving target carrying a jammer in the scenario, with a target range of 1500 m and a velocity

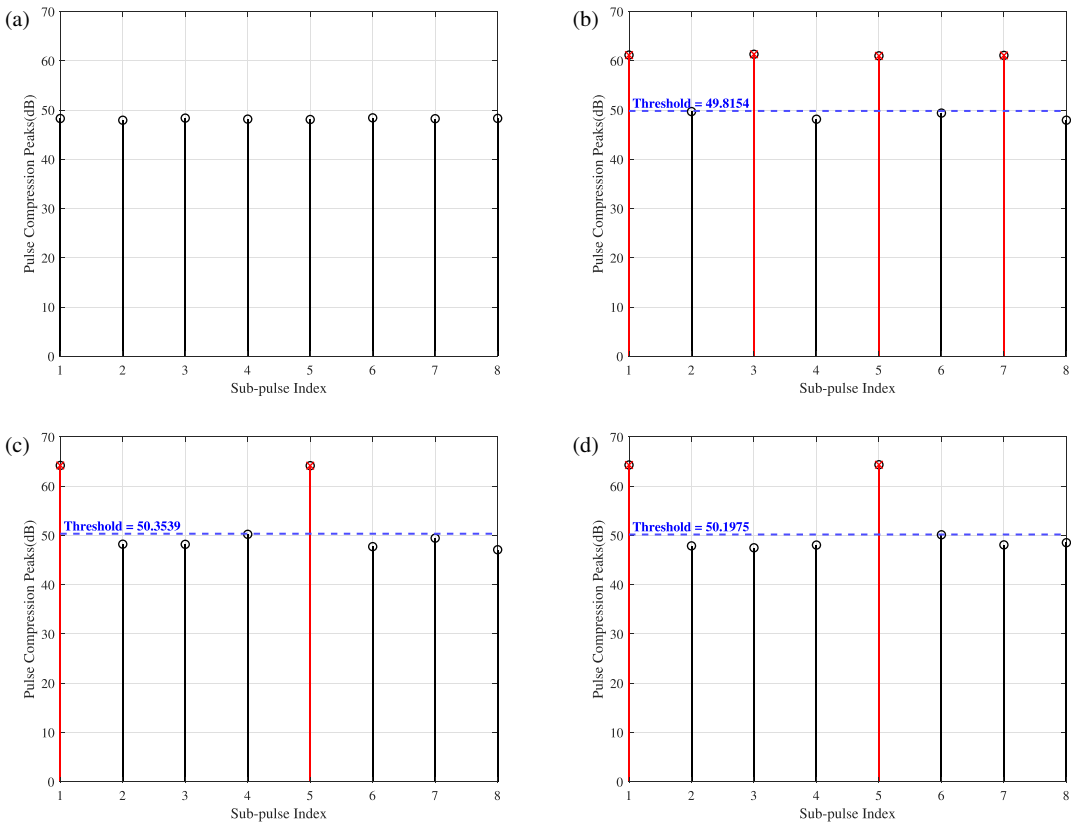

FIGURE 5. Pulse compression peak distribution of sub-pulses. (a) True target. (b) ISDRJ ($\tau = 2\,\mu s$, $T_j = 4\,\mu s$). (c) ISPRJ ($\tau = 2\,\mu s$, $T_j = 8\,\mu s$, $K = 3$). (d) ISCRJ ($\tau = 2\,\mu s$, $T_j = 8\,\mu s$, $R = 2$).

TABLE 1. Radar and interference simulation parameters.

Parameter (Unit)	Symbol	Value
Pulse width (μs)	T_p	16
Signal bandwidth (MHz)	B	64
Pulse repetition period (μs)	T_r	32
Sample rate (MHz)	f_s	128
Carrier frequency (GHz)	f_c	35
Number of subcarriers/sub-pulses	P	8
Number of chips	M	128
Interference sampling duration (μs)	τ	2
Interference sampling period (μs)	T_j	8
Signal-to-Noise Ratio (dB)	SNR	5
Jamming-to-Signal Ratio (dB)	JSR	10

of 20 m/s. The relevant simulation parameters are listed in Table 1.

5.1. ISRJ Identification

It is assumed that the jammer synchronously samples and retransmits a radar-transmitted signal. Fig. 5 illustrates the distribution of the pulse compression peaks for the sub-pulses under different scenarios. Fig. 5(a) presents the baseline scenario with a true target, where the peaks of all sub-pulses are uniform, indicating a stable response without interference. In contrast, Figs. 5(b), (c), and (d) show the scenarios for ISDRJ, ISPRJ, and ISCRJ, respectively.

As observed, the jammed sub-pulses (marked in red) exhibit significantly higher peak amplitudes than the non-jammed ones (marked in black) because of the high power and delayed forwarding of the jamming signals. This disparity creates a distinct bimodal distribution in the amplitude domain. The proposed Otsu-based method automatically calculates an optimal threshold (indicated by the blue dashed line) by maximizing between-class variance.

It is worth noting that the threshold values adaptively change across different jamming modes (e.g., 49.8154 for ISDRJ vs. 50.3539 for ISPRJ and 50.1975 for ISCRJ), demonstrating the robustness of the algorithm. The results confirm that the proposed method can accurately distinguish and classify the contaminated sub-pulses regardless of the specific jamming parameters (τ, T_j) or strategies, laying a solid foundation for subsequent interference suppression via mismatched filtering.

5.2. ISRJ Suppression

Different jamming forwarding forms result in different false target interference effects. A simulation analysis was performed for three typical types of ISRJ. The jamming suppression results of the proposed method for a single ISDRJ, ISPRJ, and ISCRJ are shown in Fig. 6. As can be seen, the peak distribution formed after pulse compression of the SSFA-MCPC signal is related to the ISRJ forwarding type, and the number of peaks corresponds to the number of forwardings.

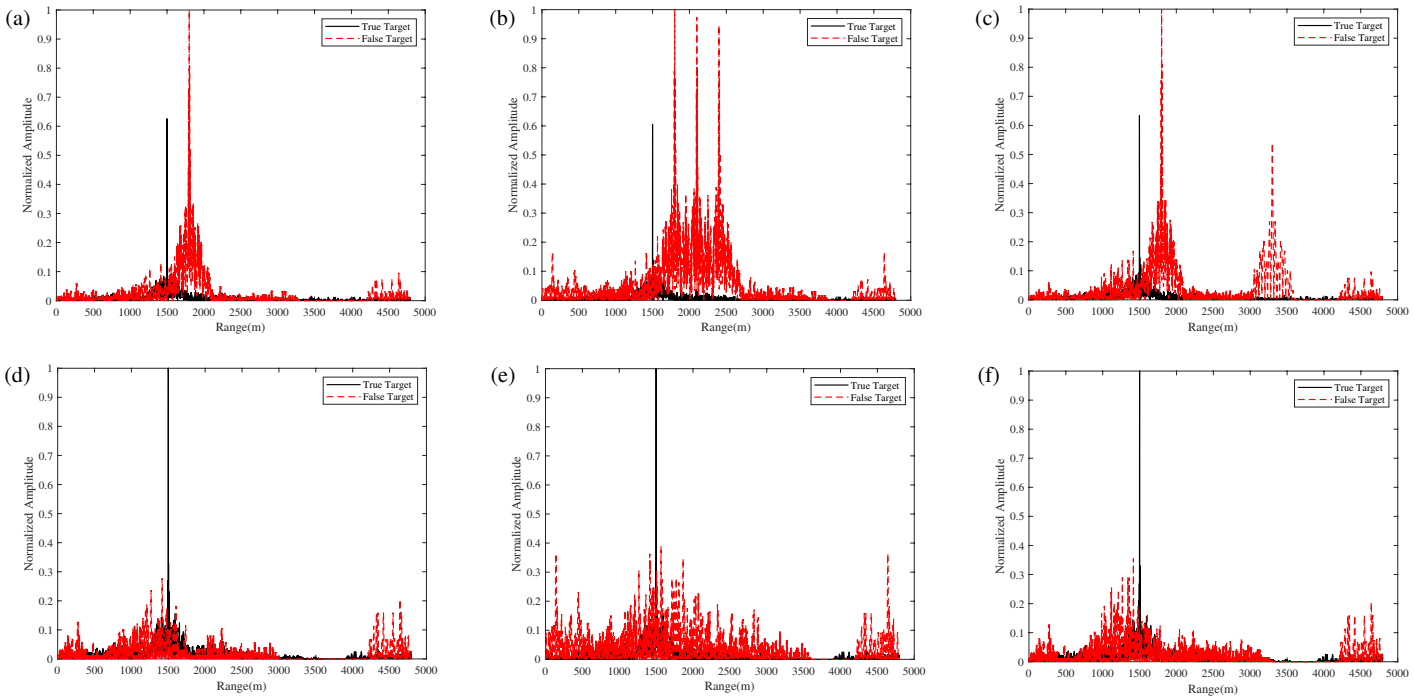

FIGURE 6. Pulse compression results of the radar echo before and after jamming suppression. (a) Before ISDRJ suppression. (b) Before ISPRJ suppression. (c) Before ISCRJ suppression. (d) After ISDRJ suppression. (e) After ISPRJ suppression. (f) After ISCRJ suppression.

Under ISDRJ conditions, the sampled signal was directly retransmitted, with a jamming duty cycle of 0.25. As shown in Fig. 6(a), before interference suppression, the ISDRJ jamming signal after pulse compression forms a strong false target, which severely affects the detection of the real target. As shown in Fig. 6(d), after applying the proposed interference suppression method, the false target signal is effectively suppressed, and no amplitude interference is introduced to the target.

Under ISPRJ conditions, with three repeated forwardings and a jamming duty cycle of 0.75, as shown in Fig. 6(b), before interference suppression, the ISPRJ jamming signal after pulse compression forms three continuous main false targets. The number of false targets increases, and their peak values are higher, leading to the suppression and deception of the real target. In contrast, as shown in Fig. 6(e), after applying the proposed interference suppression method, the amplitudes of all false target interferences are significantly reduced, and no interference in terms of amplitude or number is introduced to the target.

Under ISCRJ conditions, in addition to forwarding the sampled signal of the current cycle, previous signals were forwarded, with a maximum jamming duty cycle of 0.50. As shown in Fig. 6(c), before interference suppression, the ISCRJ jamming signal after pulse compression forms two continuous main false targets with different amplitudes. This is primarily because the ISCRJ retransmits previous signals in reverse order at different time delays. In contrast, as shown in Fig. 6(f), after applying the proposed interference suppression method, the amplitudes of the false targets are significantly reduced, and the real target becomes more prominent, allowing it to be effectively identified and extracted.

5.3. Performance Evaluation

In this subsection, the Signal-to-Jamming Ratio Improvement Factor (SJRIF) is introduced as an evaluation index for the echo pulse compression results to reflect the jamming suppression performance. The calculation formula is as follows:

$$\text{SJRIF} = \text{SJR}_a - \text{SJR}_b = 20\log\left(\frac{A_{sa}}{A_{ja}}\right) - 20\log\left(\frac{A_{sb}}{A_{jb}}\right) \quad (23)$$

where SJR_a and SJR_b represent the signal-to-jamming ratios after and before the jamming suppression, respectively. A_{sa} and A_{ja} represent the maximum amplitudes of the true and false targets after jamming suppression, respectively, whereas A_{sb} and A_{jb} represent the maximum amplitudes of the true and false targets before jamming suppression.

5.3.1. Influence of SNR on SJRIF under Different JSR Conditions

To evaluate the robustness of the proposed method against noise variations, simulation experiments were conducted to analyze the variation curves of the SJRIF under varying signal-to-noise ratio (SNR) and Jamming-to-Signal Ratio (JSR) conditions for the three forwarding modes. The number of Monte Carlo trials was 100, and the experimental results are shown in Fig. 7.

Figures 7(a), (b), and (c) illustrate the SJRIF variation with SNR for ISDRJ, ISPRJ, and ISCRJ, respectively, under different JSR conditions. The SNR before pulse compression ranged from -20 dB to 20 dB with a step size of 5 dB, while the JSR was set to 6, 9, 12, and 15 dB. It can be observed that SJRIF exhibits a positive correlation with SNR. At low SNR levels (e.g., -20 dB), the echo signal is overwhelmed by noise and is significantly affected by noise; therefore, the SJR improvement

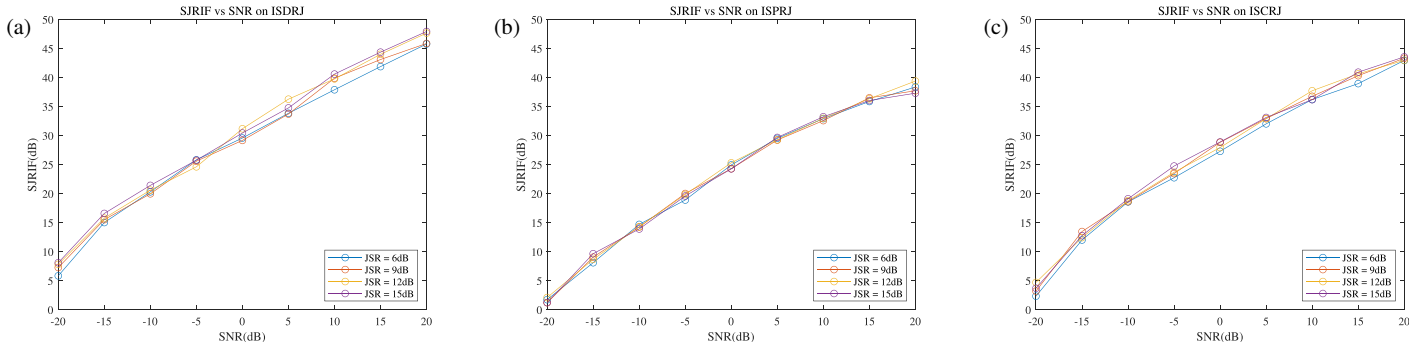

FIGURE 7. SJRIF variation with SNR under different JSR conditions. (a) SJRIF variation for ISDRJ. (b) SJRIF variation for ISPRJ. (c) SJRIF variation for ISCRJ.

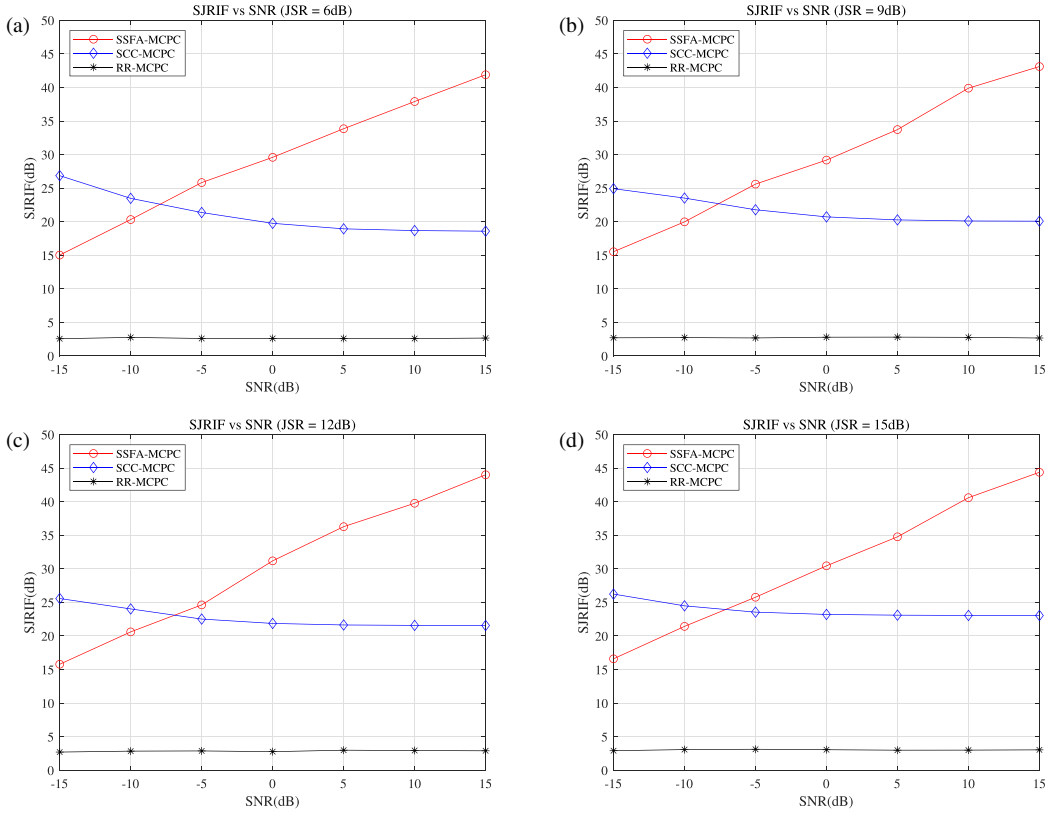

FIGURE 8. Performance comparison of different signals under different SNR and JSR conditions. (a) JSR $= 6$ dB. (b) JSR $= 9$ dB. (c) JSR $= 12$ dB. (d) JSR $= 15$ dB.

is not prominent. However, as the SNR increases, SJRIF improves steadily for all three forwarding modes. In addition, the curves corresponding to different JSR values are tightly clustered. It indicates that the proposed method is highly robust, because its improvement factor depends primarily on the noise level rather than the jamming intensity within the tested range. For ISPRJ, owing to the longer segments of the jamming signal in the retransmitted echo, it is more sensitive to noise, which slightly reduces the SJRIF, but still shows a good improvement effect.

5.3.2. Comparison with Other Radar Signals

In the signal anti-ISRJ performance evaluation experiment, the SSFA-MCPC signal designed in this paper was compared with the Random Redundancy (RR)-MCPC signal [14] and SubCarrier Cover (SCC)-MCPC signal [15] in terms of their interference suppression effects under different SNR and JSR conditions. The simulation involved 100 Monte Carlo trials, with SNR ranging from -15 to 15 dB and JSR set to 6, 9, 12, and 15 dB. The experimental results are shown in Fig. 8.

It can be seen that the proposed method exhibits a stronger anti-jamming capability than the MCPC single waveform design optimization method, specifically the RR-MCPC signal. Compared with the SCC-MCPC signal, the proposed method exhibits distinct performance characteristics based on the noise level. Under low SNR conditions (below -8 dB), the proposed method is more sensitive to noise, resulting in a lower SJRIF than that of the SCC-MCPC. However, as the SNR increases,

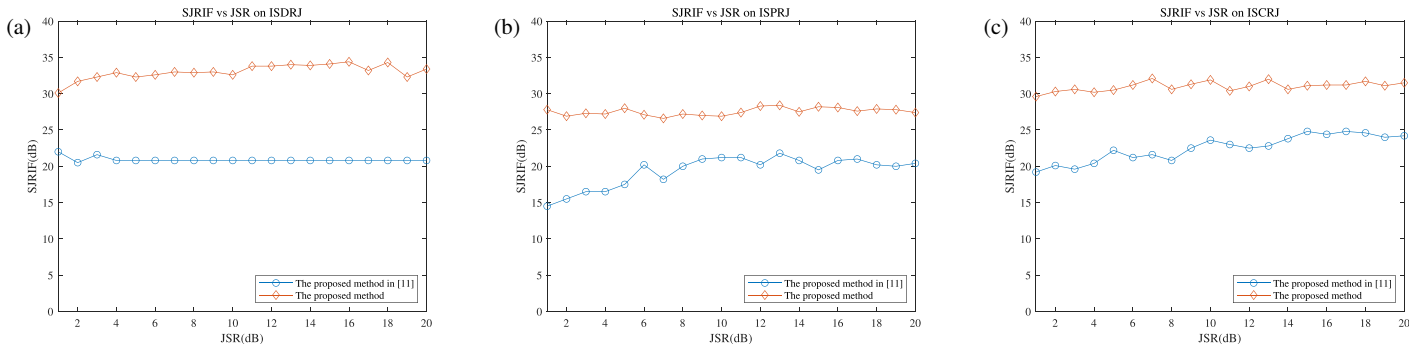

FIGURE 9. Performance comparison of different methods with different JSRs. (a) ISDRJ. (b) ISPRJ. (c) ISCRJ.

the performance of the proposed method improves rapidly. Specifically, when the SNR exceeds -5 dB, the SSFA-MCPC signal consistently outperforms the SCC-MCPC signal, achieving a much higher jamming suppression gain in high-SNR environments.

5.3.3. Comparison with Existing Method

To further demonstrate the superiority of the proposed approach, we compared its performance with that of the agile LFM-waveform-based method described in [11]. In [11], a dual-parameter agile LFM waveform is designed under known prior interference parameter conditions, where interference suppression is performed in the fractional domain using FrFT after identifying the jammed echo slices. The SJRIF variation curves with different JSRs for each method under ISDRJ, ISPRJ, and ISCRJ are shown in Fig. 9, with SNR $=$ 3 dB and JSR varying from $[1:1:20]$ dB, whereas the other parameters remain consistent.

The simulation results indicate that the proposed method maintains a significant performance advantage over that of [11]. Specifically, the proposed method yields a significant and stable SJRIF curve, demonstrating robustness against JSR variations. SJRIF remains high and fluctuates negligibly as the jamming intensity increases. In contrast, the method in [11] demonstrates noticeable instability, particularly in the ISPRJ and ISCRJ scenarios (Figs. 9(b) and (c)), indicating its sensitivity to complex jamming environments.

In the ISDRJ scenario (Fig. 9(a)), the proposed method achieves the most significant performance gain, outperforming [11] by more than 12 dB. This confirms its exceptional capability in suppressing direct repeater jamming. For ISPRJ and ISCRJ (Figs. 9(b) and (c)), SJRIF is slightly lower than ISDRJ owing to the increased sidelobes and wider false target distribution caused by repeated retransmissions. Despite this reduction, the proposed method still outperforms [11] by 7–10 dB and maintains an SJRIF within the 25–35 dB range, demonstrating good anti-jamming performance across all three forwarding modes.

Furthermore, the method in [11] is limited by accurate prior knowledge of interference parameters and is ineffective for phase-coded signals, which limits its application scenarios. In summary, the proposed anti-jamming method is more versatile, has a lower computational complexity, and is easier to implement in real-time radar systems.

However, from a practical system perspective, it should be noted that the proposed SSFA-MCPC waveform requires a relatively large instantaneous bandwidth (e.g., 64 MHz in our simulations) to achieve optimal sub-pulse orthogonality and high range resolution. Consequently, while this technique is highly suitable for specialized X and higher band radars (such as Ku- or Ka-band precision tracking and terminal-guidance radars), its implementation on typical L- or S-band surveillance radars may be limited due to bandwidth constraints, increased noise susceptibility, and reduced frequency channel availability. Despite this limitation, for high-frequency tracking radars, where ISRJ poses a severe threat, the proposed approach provides a highly effective and robust anti-jamming solution.

6. CONCLUSION

To address the threat of ISRJ, this paper integrates active and passive anti-jamming strategies and proposes an anti-jamming method based on the SSFA-MCPC signal waveform design and segmented mismatched filtering. First, the SSFA-MCPC waveform was designed by applying segmented chaotic phase coding to the MCPC signal in the time domain and introducing random frequency agility in the frequency domain. This design enhances signal randomness and mutual masking capability among sub-pulses, thereby effectively increasing the difference between the target echoes and ISRJ signals. On this basis, a segmented mismatched filtering method was developed for echo processing. By constructing a bank of sub-pulse matched filters and exploiting the pulse compression peak differences between jammed and unjammed sub-pulses, the jammer-sampled sub-pulses were adaptively identified and removed using the Otsu algorithm. The mismatched filter was then reconstructed to achieve jamming suppression. Simulation results demonstrate that the proposed method can effectively suppress three typical ISRJ modes without requiring the prior knowledge of jamming parameters, while maintaining low computational complexity. Particularly for X-band and higher band radars, this approach offers an effective solution for anti-jamming with promising engineering application potential.

ACKNOWLEDGEMENT

This work was supported in part by HuiYanXingDong (62402010206) and the Seed Fund of Research and Development Center for Multi-Sensor Intelligent Detection and Recognition Technology (ZZJJ202103-02).

REFERENCES

[1] Lewis, G. K., I. J. Bahl, E. L. Griffin, and E. R. Schineller, "GaAs MMIC's for digital radio frequency memory (DRFM) subsystems," *IEEE Transactions on Microwave Theory and Techniques*, Vol. 35, No. 12, 1477–1485, 1987.

[2] Heagney, C. P., "Digital radio frequency memory synthetic instrument enhancing US navy automated test equipment mission," *IEEE Instrumentation & Measurement Magazine*, Vol. 21, No. 4, 41–63, 2018.

[3] Wang, X., J. Liu, W. Zhang, Q. Fu, Z. Liu, and X. Xie, "Mathematic principles of interrupted-sampling repeater jamming (ISRJ)," *Science in China Series F: Information Sciences*, Vol. 50, No. 1, 113–123, 2007.

[4] Long, X., K. Li, J. Tian, J. Wang, and S. Wu, "Ambiguity function analysis of random frequency and PRI agile signals," *IEEE Transactions on Aerospace and Electronic Systems*, Vol. 57, No. 1, 382–396, 2021.

[5] Liu, Z., Y. Quan, Y. Wu, K. Xu, and M. Xing, "Range and doppler reconstruction for sparse frequency agile linear frequency modulation-orthogonal frequency division multiplexing radar," *IET Radar, Sonar & Navigation*, Vol. 16, No. 6, 1014–1025, 2022.

[6] Ding, S., C.-X. Shang, Z.-Z. Han, and H. Xie, "Continuous wave radio frequency-screen signal," *Modern Defense Technology*, Vol. 46, No. 1, 190–194, 2018.

[7] Wang, A., W. Xie, W. Chen, Y. Xiong, and Y. Wang, "Clutter and main-lobe suppression jamming suppression method for bistatic airborne radar," *Systems Engineering and Electronics*, Vol. 45, No. 3, 699–707, 2023.

[8] Zhang, J., H. Mu, S. Wen, and Y. Li, "Anti interrupted-sampling repeater jamming method based on stepped LFM waveform," *Systems Engineering and Electronics*, Vol. 41, No. 5, 1013–1020, 2019.

[9] Zhang, J., H. Mu, S. Wen, S. Liao, and M. Sha, "Anti-intermittent sampling jamming method based on intra-pulse LFM-Costas frequency stepping," *Systems Engineering and Electronics*, Vol. 41, No. 10, 2170–2177, 2019.

[10] Zhou, C., Z. Tang, F. Yu, and Y. Lu, "Anti intermittent sampling repeater jamming method based on intrapulse orthogonality," *Systems Engineering and Electronics*, Vol. 39, No. 2, 269–276, 2017.

[11] Liu, Z., Y. Quan, S. Du, Y. Wu, M. Sha, and M. Xing, "A novel ECCM scheme against interrupted-sampling repeater jamming using intra-pulse dual-parameter agile waveform," *Digital Signal Processing*, Vol. 129, 103652, 2022.

[12] Yu, T., Z. Zhou, X. Du, Q. Bao, and Y. He, "An anti-interrupted sampling repeater jamming method based on complete complementary code waveform design," *Journal of Electronics & Information Technology*, Vol. 45, No. 11, 3896–3905, 2023.

[13] Li, J., X. Luo, X. Duan, W. Wang, and J. Ou, "A novel radar waveform design for anti-interrupted sampling repeater jamming via time-frequency random coded method," *Progress In Electromagnetics Research M*, Vol. 98, 89–99, 2020.

[14] Li, J., Q. Deng, J. P. Ou, and W. Wang, "Research on random redundant multi-carrier phase code signal against ISRJ based on MIMO radar," *Progress In Electromagnetics Research M*, Vol. 110, 97–107, 2022.

[15] Li, J., J. Zhou, W. Wang, and M. Liu, "A radar waveform design of MCPC method for interrupted sampling repeater jamming suppression via fractional fourier transform," *Progress In Electromagnetics Research C*, Vol. 129, 1–15, 2023.

[16] Zhou, K., D. Li, Y. Su, and T. Liu, "Joint design of transmit waveform and mismatch filter in the presence of interrupted sampling repeater jamming," *IEEE Signal Processing Letters*, Vol. 27, 1610–1614, 2020.

[17] Wang, F., N. Li, C. Pang, C. Li, Y. Li, and X. Wang, "Complementary sequences and receiving filters design for suppressing interrupted sampling repeater jamming," *IEEE Geoscience and Remote Sensing Letters*, Vol. 19, 1–5, 2022.

[18] Qiu, X., X. Zhang, W. Jiang, and Y. Liu, "Transmit-receive joint optimization method for target measurement under interrupted sampling repeater jamming scenarios," *IEEE Transactions on Instrumentation and Measurement*, Vol. 74, 1–18, 2025.

[19] Wang, R., J. Xie, and B. Tian, "Integrated jamming perception and parameter estimation method for anti-interrupted sampling repeater jamming," *Journal of Radars*, Vol. 13, No. 6, 1337–1354, 2024.

[20] Zhou, C., Q. Liu, and X. Chen, "Parameter estimation and suppression for DRFM-based interrupted sampling repeater jammer," *IET Radar, Sonar & Navigation*, Vol. 12, No. 1, 56–63, 2018.

[21] Zhou, C., Q. Liu, and C. Hu, "Time-frequency analysis techniques for recognition and suppression of interrupted sampling repeater jamming," *Journal of Radars*, Vol. 8, No. 1, 100–106, 2019.

[22] Zhang, Y., Y. Wei, and L. Yu, "Interrupted sampling repeater jamming recognition and suppression based on phase-coded signal processing," *Signal Processing*, Vol. 198, 108596, 2022.

[23] Li, J., Y. Cao, Y. Zhang, and M. Wang, "Interrupted-sampling repeater jamming suppression based on STFrFT," *Systems Engineering and Electronics*, Vol. 46, No. 10, 3312–3324, 2024.

[24] Su, H., Q. Bao, J. Pan, F. Guo, and W. Hu, "Waveform domain adaptive matched filtering for suppressing interrupted sampling repeater jamming," *IEEE Transactions on Aerospace and Electronic Systems*, Vol. 60, No. 6, 9247–9260, 2024.

[25] Liu, Y., L. Yu, and Y. Wei, "Anti-interrupted sampling repeater jamming method based on down-sampling processing blind source separation," *Journal of Electronics & Information Technology*, Vol. 47, No. 8, 2521–2534, 2025.

[26] Deng, B., X. Wei, and X. Li, "Parameter designing of random shifted phase-coded MCPC radar signal," *Journal of National University of Defense Technology*, Vol. 33, No. 2, 68–72, 2011.

[27] Liu, L., L. Wang, Y. Yao, and X. Zhang, "Analysis of ambiguity function of combined linear frequency modulation signal," *Journal of Xi'an University of Technology*, Vol. 27, No. 4, 481–485, 2011.

[28] Xu, X., S. Xu, L. Jin, and E. Song, "Characteristic analysis of Otsu threshold and its applications," *Pattern Recognition Letters*, Vol. 32, No. 7, 956–961, 2011.